Kroflič, A., Saje, M.. Planinc, I. 2011. Non-linear analysis of two-layer beams with interlayer slip and uplift. *Computers & Structures* 89,23-24: 2414-2424 DOI: 10.1016/j.compstruc. 2011.06.007.

Non-linear analysis of two-layer beams with interlayer slip and uplift

A. Kroflič[a], M. Saje[a], I. Planinc[a,*]

[a] *University of Ljubljana, Faculty of Civil and Geodetic Engineering, Jamova 2, SI-1115 Ljubljana, Slovenia*

Abstract

A new mathematical model for the non-linear analysis of two-layer planar beams considering flexible connections is introduced and an effective, strain-based finite element numerical solution method derived. The model and the solution method account for the exact geometrically non-linear behaviour in each separate layer. Material is assumed homogeneous but can be different in each layer. The shear strains are neglected. The laws of contact in both tangent and normal directions are taken non-linear. Numerical examples verify the proposed approach. The comparisons with numerical and experimental results from literature are made and the effects of uplift on ductility and stress distribution in beams are systematically explored. The theoretical model, combined with the present numerical formulation, has been found to result in realistic behaviour, while the numerical method proves to be accurate, reliable and computationally effective.

Keywords: non-linearity, Reissner beam, slip, uplift, strain-based finite element

*Corresponding author
Email address: igor.planinc@fgg.uni-lj.si (I. Planinc)

1. Introduction

New building technologies, materials and structural elements are invented on a daily basis in civil engineering. A great deal of these inventions emerge in the field of composite structures. Yet only a profound understanding of their behaviour may lead to an optimized combination of materials, geometry and building technology.

The key in understanding the behaviour of composite structures is to perform extensive experimental and/or computational tests to assess effects of various parameters. The parameter of an utmost importance is the stiffness of the contact between the layers, which may dramatically change the mechanical performance of a structure, including its stiffness, ductility and load capacity. For that reason, much of the research in the composites attempts to find out what is the effect of the contact properties on both global and local behaviour ([1], [2], [3], [4], [5], [6]), [7], [8]). The majority of analyses have been performed by computer methods rather than experimentally.

The early numerical modelings of multi-layer composite structures date back to the middle of the previous century ([9], [10], [11], [12]). Researchers attempted to describe the partial interface connection with relatively simple mathematical models. With the increase of computer power, complex numerical models were developed for the analysis of composite beams ([8], [13], [14], [15], [16], [17]). These models neglected uplift at the contact and focused primarily on different non-linear layer material models and contact slip laws ([18], [19], [20], [21], [22], [23], [24], [25], [26]). The models based on the geometrically non-linear beam theory have been very rarely discussed ([1], [21], [27], [28]). The particular examples studying the effect of slip on the buckling capacity of two-layer composite beams are given in ([6], [29], [30]).

Adekola [13] was probably the first to discuss analytically the combined effect of both slip and uplift on the behaviour of two-layer composite beams. Robinson and Naraine [3] presented the solution in the form of explicit expressions of a somewhat modified Adekola's system of differential equations. The above

mentioned authors considered only a geometrically and materially linear model. The models that account for a bilinear or fully non-linear contact model for the uplift have been given only recently, see ([31], [32], [33]).

When employing a finite element type of numerical solution, one has to select the optimal set of basic variables of the problem. There are several solutions available that consider displacement-based formulations ([20], [31], [34]). Salari et al. [5] and Ayoub [2] considered a finite element formulation based on the force interpolation. Dall'Asta and Zona [35] and Ayoub and Filippou [36] employed mixed elements, where both the displacements and forces have been interpolated.

Here a new finite element formulation for fully geometrically and materially non-linear analysis of two-layer beams is presented whose basic variables are strains. Hence, the only unknown functions of the formulation are strains. The Galerkin-type of the finite element formulation is employed as in Planinc et al. [37]. The mathematical model of the composite beam considers the following assumptions: the composite structure, an external loading and deformations are planar; the material of each layer is taken to be non-linear and homogeneous, yet it can differ from layer to layer; the geometrically and materially non-linear Reissner's beam theory is assumed for each layer; shear strains are neglected.

After the new formulation has been set up, the numerical solution of the present model is compared with the Girhammar and Gopu analytical solution, derived from the second-order geometrically non-linear theory [38], and with the experimental results by Ansourian [39] to validate our model. Finally, the effect of the choice of the uplift constitutive law on the global response is presented and discussed.

2. Basic equations of a two-layer beam

The set of governing equations of a two-layer beam with the interlayer slip and uplift being taken into account consists of kinematic, equilibrium and constitutive equations supplemented by the proper natural and essential boundary

conditions of each layer. Bonded behaviour of the layers is dictated by proper constraining conditions [1].

2.1. Kinematic, equilibrium and constitutive equations

A planar, two-layer, geometrically and materially non-linear beam of inital length L is assumed here. The generalization of equations from a two-layer beam to a multi-layer one can be derived in a similar way.

Fig. 1 presents the undeformed and deformed configurations of a two-layer beam. The beam consists of the bottom layer, henceforth called layer a, and the upper layer, called layer b. The layers have constant cross-sections A^a and A^b along the length. We assume that the connection between the layers is flexible enough to allow for some slip and uplift between the layers.

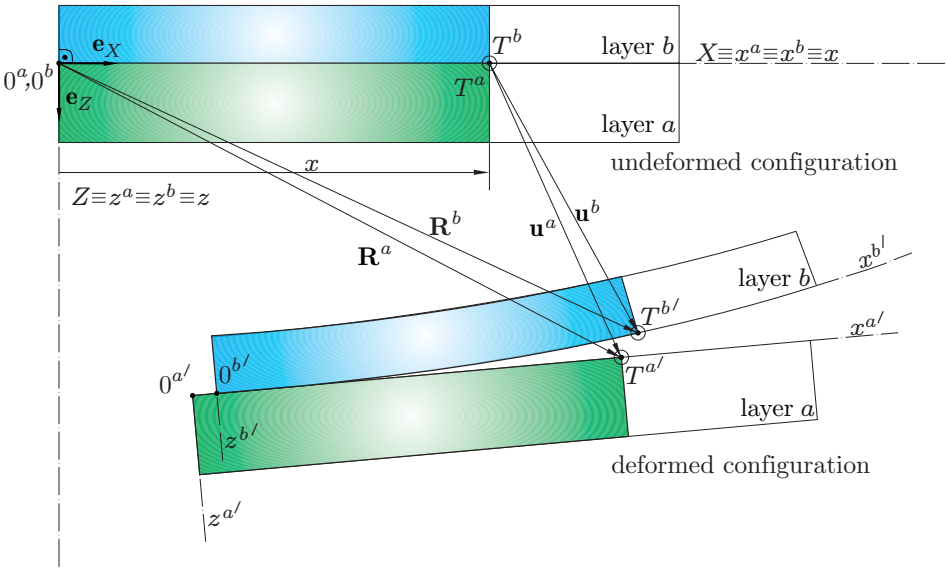

Figure 1: Undeformed and deformed configurations of a two-layer beam.

Large displacements of each layer are assumed, so that the geometrically non-linear beam model is necessary. Behaviour of the beam is assumed to be planar in the (X, Z)-plane of a fixed spatial Cartesian coordinate system (X, Y, Z) with base vectors $\mathbf{e}_X$, $\mathbf{e}_Y$, $\mathbf{e}_Z$, where $\mathbf{e}_Y = \mathbf{e}_Z \times \mathbf{e}_X$. Each layer

is additionally parametrized by its own material coordinate system placed on the contact of the layers so that the two coordinate systems coincide in the undeformed configuration: $x^a \equiv x^b \equiv x$, $y^a \equiv y^b \equiv y$, $z^a \equiv z^b \equiv z$. In what follows the material axes $x^a \equiv x^b \equiv x$ will be termed the 'reference axes'. Furthermore, we take that the undeformed axes of the material coordinate systems initially coincide with the spatial coordinate axes (X, Y, Z) such that $x \equiv X$, $y \equiv Y$, $z \equiv Z$.

The position vector of a material point $(x, 0, 0)$ on the deformed reference axes of the two layers is defined by $(i = a, b)$

$$\mathbf{R}^i = x\ \mathbf{e}_X + \mathbf{u}^i = \left(x + u^i\right) \mathbf{e}_X + w^i \mathbf{e}_Z, \tag{1}$$

where $(\bullet)^i$ denotes quantities related to layers a and b, respectively. u^i, w^i in Eq. (1) denote the X– and Z–components of the displacement vectors of the material point $(x,\ 0,\ 0)$ of the reference axes of the layers.

Bernoulli's hypothesis of planar cross-sections that the plane cross-section of each layer remains planar and perpendicular to its deformed axis is assumed for each layer. This leads to Reissner's [40] exact, shear-stiff non-linear kinematic equations $(i = a, b)$

$$\begin{aligned} 1 + u^{i\prime} - \left(1 + \varepsilon^i\right) \cos\varphi^i &= 0, \\ w^{i\prime} + \left(1 + \varepsilon^i\right) \sin\varphi^i &= 0, \\ \varphi^{i\prime} - \kappa^i &= 0, \end{aligned} \tag{2}$$

where ε^i denotes extensional strains, κ^i curvatures, and φ^i rotations of the reference axes of layers a and b. The prime represents the derivative with respect to x. Note that the effect of shear strains is neglected in the above equations. According to Bernoulli's hypothesis, the extensional strain, D^i $(i = a, b)$, of an arbitrary axial fibre of layer a or b is a linear function of the sectional coordinate z:

$$D^i = \varepsilon^i + z\kappa^i. \tag{3}$$

The equilibrium equations relate the equilibrium internal forces R_X^i, R_Z^i and M^i of layers i with the distributed line loads q_X^i, q_Z^i, m_Y^i, p_X^i, p_Z^i [19] (Fig. 2):

$$\begin{aligned} R_X^{i\prime} + q_X^i + p_X^i &= 0, \\ R_Z^{i\prime} + q_Z^i + p_Z^i &= 0, \\ M^{i\prime} - \left(1+\varepsilon^i\right) Q^i + m_Y^i &= 0, \end{aligned} \tag{4}$$

where R_X^i, R_Z^i, p_X^i, p_Z^i, q_X^i and q_Z^i are the X– and Z–components of the equilibrium internal forces, the contact traction vector, and the external distributed line loads, respectively. The forces R_X^i, R_Z^i $(i = a, b)$ are related to the layer equilibrium axial forces N^i and shear forces Q^i with respect to the rotated cross-section by

$$\begin{aligned} N^i &= R_X^i \cos\varphi^i - R_Z^i \sin\varphi^i, \\ Q^i &= R_X^i \sin\varphi^i + R_Z^i \cos\varphi^i. \end{aligned} \tag{5}$$

M^i and m_Y^i are the cross-sectional equilibrium bending moment and the external line moment traction, respectively. The final set of equations concern the constitutive equations and is called the consistency conditions. They require that the internal equilibrium and the internal constitutive axial forces and moments are equal over each cross-section on the reference axis. Satisfying these conditions results in four equations, which relate the equilibrium-satisfying forces N^i, M^i to the constitutive forces N_c^i, M_c^i obtained as the stress-resultants of the normal stress, σ^i, over the cross-section of layer i:

$$\begin{aligned} N^i = N_c^i &= \int_{A^i} \sigma^i\left(D^i\right) dA, \\ M^i = M_c^i &= \int_{A^i} z^i \sigma^i\left(D^i\right) dA. \end{aligned} \tag{6}$$

$\sigma^i\left(D^i\right)$ is a function of the extensional strain D^i in the fibre z of layer i. The constitutive quantities, N_c^i, M_c^i, depend on a chosen material model defined by the relationship $\sigma^i = \sigma^i\left(D^i\right)$ to be determined experimentally. Note that N_c^i and M_c^i are the stress-resultants of the normal stress over the cross-section of layer i with respect to the coordinate system (y, z) whose null point is not coincident with the geometrical centre of the layer.

The presented system of equations cannot be solved uniquely without considering the appropriate natural and essential boundary conditions which, for the problem at hand, takes the form:

$x = 0$:

$$\begin{aligned} R_X^i(0) + S_1^i &= 0, & u^i(0) &= u_1^i, \\ R_Z^i(0) + S_2^i &= 0, \quad \text{or} & w^i(0) &= u_2^i, \\ M^i(0) + S_3^i &= 0, & \varphi^i(0) &= u_3^i; \end{aligned} \tag{7}$$

$x = L$:

$$\begin{aligned} -R_X^i(L) + S_4^i &= 0, & u^i(L) &= u_4^i, \\ -R_Z^i(L) + S_5^i &= 0, \quad \text{or} & w^i(L) &= u_5^i, \\ -M^i(L) + S_6^i &= 0, & \varphi^i(L) &= u_6^i. \end{aligned} \tag{8}$$

In the above equations, u_m^i $(m = 1, ..., 6)$ denote the prescribed boundary displacements, whereas S_m^i $(m = 1, ..., 6)$ are the prescribed complementary boundary forces at $x = 0$ and $x = L$ of layers a and b.

2.2. Constraining equations

It is clear that two bodies transmit forces when they are in contact. When considering a geometrically non-linear problem, it is not suitable to relate the constraining equations in the $\mathbf{e}_X$ and $\mathbf{e}_Z$ directions, as is standard for the geometrically linearized models ([8], [13], [14], [15], [16], [17]). Instead, we introduce a so-called 'mean contact surface (or line)' whose normal and tangential vectors, $\mathbf{e}_n^*$ and $\mathbf{e}_t^*$, at the point of contact are defined as [41] (see Fig. 2):

$$\begin{aligned} \mathbf{e}_n^* &= \frac{\zeta \mathbf{e}_n^a + (1-\zeta)\,\mathbf{e}_n^b}{||\zeta \mathbf{e}_n^a + (1-\zeta)\,\mathbf{e}_n^b||} = e_{nX}^* \mathbf{e}_X + e_{nZ}^* \mathbf{e}_Z, \\ \mathbf{e}_t^* &= \frac{\zeta \mathbf{e}_t^a + (1-\zeta)\,\mathbf{e}_t^b}{\left|\left|\zeta \mathbf{e}_t^a + (1-\zeta)\,\mathbf{e}_t^b\right|\right|} = e_{tX}^* \mathbf{e}_X + e_{tZ}^* \mathbf{e}_Z. \end{aligned} \tag{9}$$

Here ζ represents the weight with some value between $[0, 1]$, $\mathbf{e}_n^i$ $(i = a, b)$ represents the deformed normal and $\mathbf{e}_t^i$ the deformed tangent of the contact

point on the surfaces of layers a and b. The norm $||\bullet||$ is the length of the vector, and e^*_{nX}, e^*_{nZ}, e^*_{tX}, e^*_{tZ} denote the X– and Z–components of the unit vectors $\mathbf{e}^*_n$ and $\mathbf{e}^*_t$. If not stated otherwise $\zeta = 0.5$ is taken to determine the mean normal and tangential vectors of the deformed mean contact surface. It should be also pointed out that $\mathbf{e}^*_n$ and $\mathbf{e}^*_t$ in Eq. (9) cannot be uniquely determined when $\mathbf{e}^a_n = -\mathbf{e}^b_n$ and/or $\mathbf{e}^a_t = -\mathbf{e}^b_t$. This condition, however, represents no limitation in solving practical problems. The action-reaction law between the contact

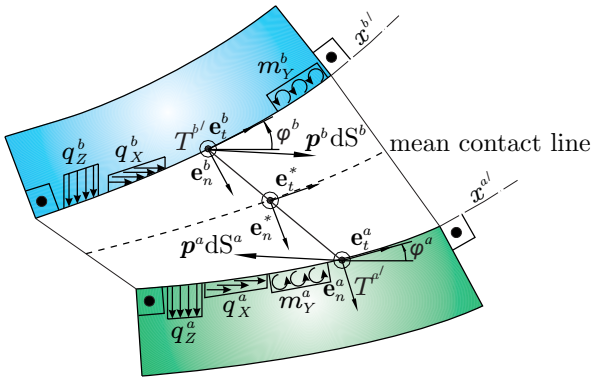

Figure 2: Geometrical meaning of the normal and the tangent to the mean contact line. Description of contact and external tractions.

surfaces requires that the contact tractions satisfy the equilibrium condition

$$\boldsymbol{p}^a \mathrm{dS}^a + \boldsymbol{p}^b \mathrm{dS}^b = \mathbf{0}, \tag{10}$$

where $\boldsymbol{p}^a \mathrm{dS}^a$ and $\boldsymbol{p}^b \mathrm{dS}^b$ represent the contact forces (Fig. 2). After considering the assumption that $\mathrm{dS}^a = \mathrm{dS}^b$, we can write

$$\boldsymbol{p}^a + \boldsymbol{p}^b = \mathbf{0}. \tag{11}$$

To simplify the notation, we further introduce $\boldsymbol{p}$ as

$$\boldsymbol{p} = \boldsymbol{p}^a = -\boldsymbol{p}^b = p_X \mathbf{e}_X + p_Z \mathbf{e}_Z, \tag{12}$$

where p_X, p_Z denote the components of $\boldsymbol{p}$ with respect to the spatial coordinate system per unit of initial length. They can also be expressed with respect to

the mean basis:

$$p_X = p_t^* e_{tX}^* + p_n^* e_{nX}^*, \qquad p_Z = p_t^* e_{tZ}^* + p_n^* e_{nZ}^*, \tag{13}$$

where p_t^* is the component of the contact traction force along the vector $\mathbf{e}_t^*$, while p_n^* is its component along the vector $\mathbf{e}_n^*$.

Similarly, the components of the displacement vectors $\mathbf{u}^i$ with respect to the mean base vectors ($i = a, b$) take the form

$$w_n^{i*} = \mathbf{u}^i \cdot \mathbf{e}_n^*,$$
$$u_t^{i*} = \mathbf{u}^i \cdot \mathbf{e}_t^*.$$

Mean uplift, d^*, and mean slip, Δ^*, are defined as

$$\Delta^* = u_t^{a*} - u_t^{b*}, \qquad d^* = w_n^{a*} - w_n^{b*}. \tag{14}$$

According to Alfano and Crisfield [33], there are roughly two models available to formulate the contact constitutive relationship. The coupled (mixed) model is capable of considering the mixed mode delamination with simultaneous opening and sliding processes as a coupled act. Consequently, there the contact traction components are assumed dependent on both d^* and Δ^*, so that a rather general constitutive law is possible to be defined as

$$p_t^* = F\left(\Delta^*, d^*\right), \qquad p_n^* = G\left(\Delta^*, d^*\right). \tag{15}$$

As having in mind structural engineering applications, we here consider only an uncoupled model of the contact constitutive relationship, which has already been used by, e.g. Adekola [13] and Gara et al. [31]. This model assumes an independent behaviour in each direction, which is expressed as

$$p_t^* = F\left(\Delta^*\right), \qquad p_n^* = G\left(d^*\right). \tag{16}$$

It is worth mentioning that a consistent linearization of Eqs. (13) and (14) around an undeformed configuration and the consideration of (16) results in the simplified relationships

$$\Delta^* = \Delta = u^a - u^b, \qquad d^* = d = w^a - w^b, \tag{17}$$

$$p_t^* = p_X = F\left(\Delta\right), \qquad p_n^* = p_Z = G\left(d\right), \tag{18}$$

which have been derived in [15] already.

For given data, i.e. geometry of the beam, external loadings, boundary conditions and material parameters, Eqs. (2), (4), (5), (6), (14), (16) constitute a system of 26 differential and algebraic equations for 26 unknown functions u^a, u^b, w^a, w^b, φ^a, φ^b, ε^a, ε^b, κ^a, κ^b, R_X^a, R_X^b, R_Z^a, R_Z^b, N^a, N^b, Q^a, Q^b, M^a, M^b, Δ^*, d^*, p_t^{a*}, p_t^{b*}, p_n^{a*}, p_n^{b*} with the corresponding natural and essential boundary conditions (7)–(8).

3. The finite element formulation

The introduction of an exact analytical solution of the stress-strain state of a composite beam is possible only in the rare cases such as is the case of linear models (Adekola [13], Robinson and Naraine [3], Kroflič et al. [15]). In order to obtain the solution of non-linear models of much more complexity, we have to adress approximative numerical methods. In the present paper the above given equations will be solved numerically by the strain-based finite element method ([1], [19]). To that end we first introduce a modified principle of virtual work, in which the deformations become the only unknown functions of the problem (Planinc et al. [37]). The remaining unknowns are involved in the functional only through their boundary values. The modified principle of virtual work reads

$$
\begin{aligned}
\delta W^{*} = & \sum_{i=a}^{b} \delta W^{i*} = \\
& \sum_{i=a}^{b} \int_{0}^{L} \left(\left(N_c^i - N^i \right) \delta \varepsilon^i + \left(M_c^i - M^i \right) \delta \kappa^i \right) dx^i + \\
& + \left(u^i \left(L \right) - u^i \left(0 \right) - \int_{0}^{L} \left(\left(1 + \varepsilon^i \right) \cos \varphi^i - 1 \right) d\xi \right) \delta R_X^i(0) + \\
& + \left(w^i \left(L \right) - w^i \left(0 \right) + \int_{0}^{L} \left(\left(1 + \varepsilon^i \right) \sin \varphi^i \right) d\xi \right) \delta R_Z^i(0) + \\
& + \left(\varphi^i \left(L \right) - \varphi^i \left(0 \right) - \int_{0}^{L} \kappa^i d\xi \right) \delta M^i \left(0 \right) + \\
& + \left(-S_1^i - R_X^i \left(0 \right) \right) \delta u^i \left(0 \right) + \left(-S_2^i - R_Z^i \left(0 \right) \right) \delta w^i \left(0 \right) + \\
& + \left(-S_3^i - M^i \left(0 \right) \right) \delta \varphi^i \left(0 \right) + \left(-S_4^i + R_X^i \left(L \right) \right) \delta u^i \left(L \right) + \\
& + \left(-S_5^i + R_Z^i \left(L \right) \right) \delta w^i \left(L \right) + \left(-S_6^i + M^i \left(L \right) \right) \delta \varphi^i \left(L \right) = 0.
\end{aligned}
\tag{19}
$$

As observed from Eq. (19), the principle depends on deformation functions $\varepsilon^a(x)$, $\varepsilon^b(x)$, $\kappa^a(x)$ and $\kappa^b(x)$, boundary forces $R_X^a(0)$, $R_Z^a(0)$, $M^a(0)$, $R_X^b(0)$, $R_Z^b(0)$, $M^b(0)$, and boundary displacements and rotations $u^a(0)$, $u^a(L)$, $w^a(0)$, $w^a(L)$, $\varphi^a(0)$, $\varphi^a(L)$, $u^b(0)$, $u^b(L)$, $w^b(0)$, $w^b(L)$, $\varphi^b(0)$ and $\varphi^a(L)$ at $x = 0$ and $x = L$.

In order to discretize Eq. (19), the interpolation functions for deformations ε^a, ε^b, κ^a and κ^b have to be introduced. The variation of extensional and bending strains of layers with x are approximated by the interpolation ($i = a, b$):

$$
\begin{aligned}
\varepsilon^i \left(x \right) &= \sum_{m=1}^{M} L_m \left(x \right) \varepsilon_m^i, \\
\kappa^i \left(x \right) &= \sum_{m=1}^{M} L_m \left(x \right) \kappa_m^i,
\end{aligned}
\tag{20}
$$

where L_m $(m = 1, 2, ..., M)$ are the Lagrangian polynomials of order $(M - 1)$; M is the number of interpolation points, and index m denotes the interpolation point at $x = x_m$; $\varepsilon_m^i = \varepsilon^i(x_m)$, $\kappa_m^i = \kappa^i(x_m)$ are the strains at x_m. The

interpolation points along the finite element are taken to be equidistant, $x_m = \frac{L}{M-1}m$. Following the interpolation in Eqs. (20), we derive the same expressions for the variations of the deformation quantities as

$$\delta\varepsilon^i(x) = \sum_{m=1}^{M} L_m(x)\,\delta\varepsilon_m^i, \qquad (21)$$
$$\delta\kappa^i(x) = \sum_{m=1}^{M} L_m(x)\,\delta\kappa_m^i.$$

When we insert the interpolated functions into the modified principle of virtual work, the coefficients at the independent variations of functional (19) must equal to zero resulting in the following system of discrete equilibrium Euler–Lagrangian equations of a two-layer composite beam accounting for an interlayer slip and uplift:

$$g_m = \int_0^L \left(N_c^a - N^a\right) L_m \, dx = 0, \qquad m = 1, ..., M$$

$$g_{M+m} = \int_0^L \left(N_c^b - N^b\right) L_m \, dx = 0, \qquad m = 1, ..., M$$

$$g_{2M+m} = \int_0^L \left(M_c^a - M^a\right) L_m \, dx = 0, \qquad m = 1, ..., M$$

$$g_{3M+m} = \int_0^L \left(M_c^b - M^b\right) L_m \, dx = 0, \qquad m = 1, ..., M$$

$$g_{4M+1} = u^a(L) - u^a(0) - \int_0^L \left(\left(1+\varepsilon^a\right)\cos\varphi^a - 1\right) dx = 0,$$

$$g_{4M+2} = w^a(L) - w^a(0) + \int_0^L \left(\left(1+\varepsilon^a\right)\sin\varphi^a\right) dx = 0,$$

$$g_{4M+3} = \varphi^a(L) - \varphi^a(0) - \int_0^L \kappa^a dx = 0,$$

$$g_{4M+4} = u^b(L) - u^b(0) - \int_0^L \left(\left(1+\varepsilon^b\right)\cos\varphi^b - 1\right) dx = 0,$$

$$g_{4M+5} = w^b(L) - w^b(0) + \int_0^L \left(\left(1+\varepsilon^a\right)\sin\varphi^a\right) dx = 0,$$

$$g_{4M+6} = \varphi^b(L) - \varphi^b(0) - \int_0^L \kappa^b dx = 0, \tag{22}$$

$$g_{4M+7} = -S_1^a - R_X^a(0) = 0,$$

$$g_{4M+8} = -S_2^a - R_Z^a(0) = 0,$$

$$g_{4M+9} = -S_3^a - M^a(0) = 0,$$

$$g_{4M+10} = -S_1^b - R_X^b(0) = 0,$$

$$g_{4M+11} = -S_2^b - R_Z^b(0) = 0,$$

$$g_{4M+12} = -S_3^b - M^b(0) = 0,$$

$$g_{4M+13} = S_4^a - R_X^a(L) = 0,$$

$$g_{4M+14} = S_5^a - R_Z^a(L) = 0,$$

$$g_{4M+15} = S_6^a - M^a(L) = 0,$$

$$g_{4M+16} = S_4^b - R_X^b(L) = 0,$$

$$g_{4M+17} = S_5^b - R_Z^b(L) = 0,$$

$$g_{4M+18} = S_6^b - M^b(L) = 0.$$

The system of Eqs. (22) constitutes an algebraic system of $4M+18$ discrete governing equations of the two-layer composite beam for $4M+18$ primary unknowns. These consist of $4M+6$ internal degrees of freedom, ε_m^i, κ_m^i $(m=1,2,...,M)$, and $R_X^i(0)$, $R_Z^i(0)$, $M^i(0)$, and 12 classical external degrees of freedom, $u^i(0)$, $w^i(0)$, $\varphi^i(0)$, $u^i(L)$, $w^i(L)$, $\varphi^i(L)$ of a composite beam finite element. The secondary unknown functions, u^i, w^i, φ^i, R_X^i, R_Z^i, M^i , Δ^*, d^*, p_t^{a*}, p_n^{a*}, p_t^{b*}, p_n^{b*}, when needed at a particular value of x in the above Eqs. (22), are obtained by the equations

$$
\begin{aligned}
u^i(x) &= u^i(0) + \int_0^x \left(\left(1+\varepsilon^i\right)\cos\varphi^i - 1\right) d\xi, \\
w^i(x) &= w^i(0) - \int_0^x \left(\left(1+\varepsilon^i\right)\sin\varphi^i\right) d\xi, \\
\varphi^i(x) &= \varphi^i(0) + \int_0^x \kappa^i d\xi, \\
R_X^i(x) &= R_X^i(0) - \int_0^x \left(q_X^i + p_X^i\right) d\xi, \\
R_Z^i(x) &= R_Z^i(0) - \int_0^x \left(q_Z^i + p_Z^i\right) d\xi, \\
M^i(x) &= M^i(0) + \int_0^x \left(\left(1+\varepsilon^i\right) Q^i - m_Y^i\right) d\xi, \\
d^*(x) &= w_n^{a*} - w_n^{b*}, \\
\Delta^*(x) &= u_t^{a*} - u_t^{b*}, \\
p_t^{a*}(x) &= -p_t^{b*}(x) = F\left(\Delta^*\right), \\
p_n^{a*}(x) &= -p_n^{b*}(x) = G\left(d^*\right).
\end{aligned}
\tag{23}
$$

After the boundary conditions have been inserted in the system, the incremental-iterative Newton–Raphson method is employed for the solution of the assembled system of the discrete equations of the structure.

4. Numerical examples

Our first numerical examples verify the proposed approach. Only then we validate our numerical model against the numerical and experimental results

from literature [39].

4.1. Verification of the mathematical model

The present numerical model is verified:

- by comparing numerical results of the present model with the analytical solution of Girhammar and Gopu [38],
- by studying p- and h-convergence of the numerical results of a simply supported, elastic, two-layer beam, and
- by studying p- and h-convergence of the numerical results of a geometrically and materially non-linear two-layer timber beam.

Girhammar and Gopu [38] presented exact solutions of the first- and second-order theories for the stress and strain state of a simply supported elastic composite beam with the partial interaction only in the tangential direction. The data of the beam are given in Fig. 3 where K and C denote the linearized contact stiffnesses in the axial and transverse direction. A nearly rigid connection ($C = 1000$ kN/cm^2) in the normal direction, $\mathbf{e}_n^*$, has been considered in the present verification.

The comparison between the present numerical and Girhammar's analytical results [38] is displayed in Table 1. The numerical results have been obtained with the use of 2 finite elements E_5 (5 interpolation and 5 integration points along the axis of the finite element, see [37] for a detailed description of the strain-based finite elements). The results of the geometrically linear beam model as obtained by Kroflič et al. [42] are also shown in Table 1.

An excellent accuracy of the present results for both geometrically linear and geometrically non-linear theory can be observed with the use of only two finite elements E_5.

Our further verification step comprises analyses of p- and h-convergence of the method. The effects of the number of elements, the degree of interpolation and the order of numerical integration on the accuracy of the results are presented in two verification cases. Geometry, loading and material properties of

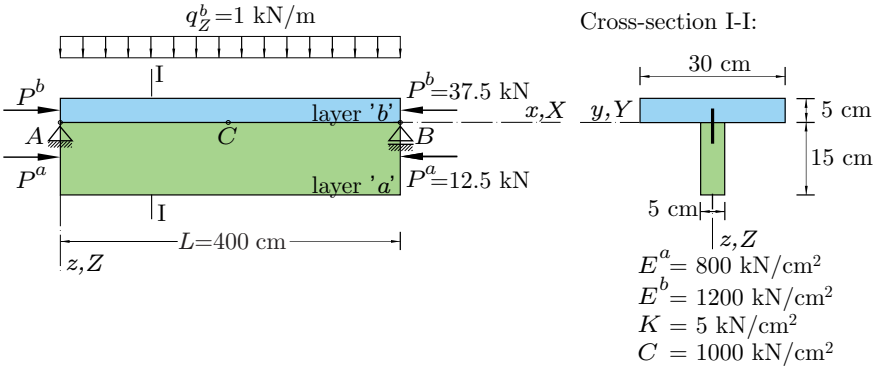

Figure 3: Loading, geometrical and material data of the Girhammar and Gopu beam [38].

Table 1: Analytical [38] and numerical results of a simply supported linear elastic composite beam.

	Analytical [38]		2 FE E_5	
quantity	GLT[1]	MSOT[2]	GLT[3]	GNT[4]
w_C^a [mm]	7.560	9.276	7.560	9.273
N_C^a [kN]	0.863	3.897	0.862	3.927
N_C^b [kN]	–50.863	–53.897	–50.862	–53.927
M_C^a [kNm]*	0.4977	0.6162	0.4978	0.6136
M_C^b [kNm]*	0.1659	0.2054	0.1659	0.2069
$p_{t,A}^*$ [kN/cm]	11.444	13.878	11.447	13.858

[1] Geometrically linear theory [38]

[2] Modified second-order theory [38]

[3] Geometrically linear theory [42]

[4] Geometrically non-linear theory (present)

* Bending moment with respect to the centroidal line of the layer

the first, linear elastic, yet geometrically non-linear verification case, i.e. a fully clamped, two-layer beam, are displayed in Fig. 4.

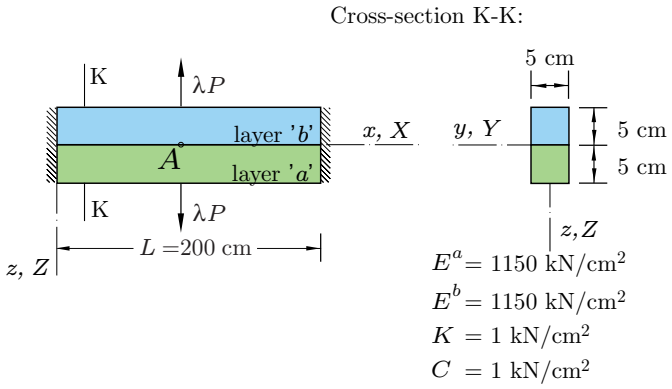

Figure 4: Loading, geometrical and material data of a fully clamped beam.

We measure convergence of finite elements using the relative error, defined as

$$\text{error}_w = \frac{w^a_{A,20,E_6} - w^a_{A,k}}{w^a_{A,20,E_6}} 100\%, \tag{24}$$

where $w^a_{A,20,E_6}$ denotes the vertical displacement of layer a at the beam midspan (point A) for a 20 E_6 finite-element mesh, and $w^a_{A,k}$ is the vertical displacement for a k finite-element mesh. The results of the 20 E_6 finite-element mesh are taken as the reference results whose absolute error is far less than a promile.

The convergence of displacement w^a_A is shown in Fig. 5 for two load levels, $\lambda = 25$ and $\lambda = 900$ ($P = 10$ kN), and for finite elements of various degrees, N=2 ,..., 6. In element E_N, the N-point Gaussian integration was employed.

A substantial decrease in error always occurs with an increase of the number of finite elements. The solutions applying a high degree polynomial interpolation are highly accurate even with the use of a small number of finite elements. For example, the relative error of the vertical displacement, w^a_A, when evaluated with four finite elements E_5, is roughly 0.12% for $\lambda = 25$ (Fig. 5(a)) and 0.55% for $\lambda = 900$ (Fig. 5(b)). The deformed shapes of the beam are presented in Fig. 6 for load levels $\lambda = 25$, 50 and 900. Note a large value of the central deflection of the two layers of the beam as well as their large uplift.

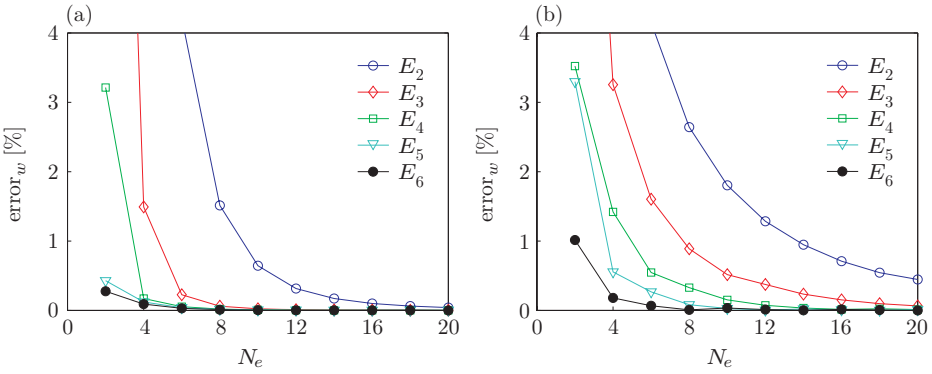

Figure 5: The relative error of vertical displacement w_A vs. number of elements for load level (a) $\lambda = 25$ and (b) $\lambda = 900$.

In our second verification case, we consider both geometrical and material non-linearity. A timber, two-span continuous beam is analysed. The overall length of the beam is $L = 600$ cm, while the spans are $L_1 = \frac{2}{3}L = 400$ cm and $L_2 = \frac{1}{3}L = 200$ cm. Loading and geometrical data of the beam are given in Fig. 7. Timber rafters are connected to each other with standard nails 40/100 in two rows. The axial distance between the nails is 6 cm. Please observe that only the bottom layer of the composite beam is supported (Fig. 7).

The non-linear stress-strain relationship of timber proposed by Pischl [43] (Fig. 8) is assumed with the values of material parameters as follows: $D_{c,e} = -200/85$ ‰, $D_{c,f} = -6.5$ ‰, $D_{t,f} = 32/10$ ‰, $f_{c,f} = -2.88$ kN/cm^2, $f_{t,f} = 2.56$ kN/cm^2 and $E_c = E_t = 800$ kN/cm^2. The non-linear mean slip (Δ^*) – traction force (p_t^*) relationship and the corresponding uplift (d^*) – traction force (p_n^*) relationship are taken from [44], see Figs. 9(a) and 9(b) for their graphs. The convergence analysis is made firstly for a nearly rigid normal connection, assuming a big number $C = 1000$ kN/cm^2, and only then the realistic non-linear relationship shown in (Fig. 9(b)) is considered.

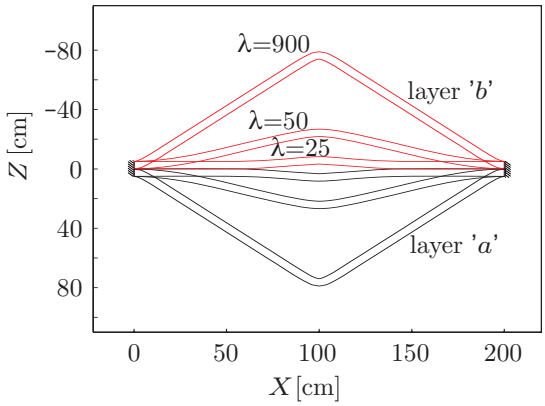

Figure 6: The actual deformed shapes of a fully clamped beam for load levels $\lambda = 25,\ 50$ and 900.

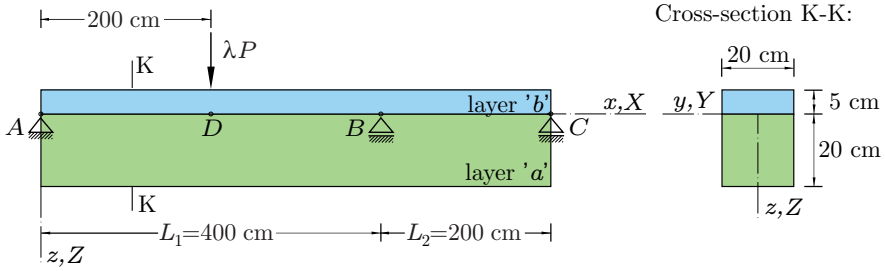

Figure 7: Loading and geometrical data of continuous beam.

The measure of convergence of finite elements is again defined to be the relative error of the deflection

$$\text{error}_w = \frac{w^a_{A,21} - w^a_{A,k}}{w^a_{A,21}} 100\%, \tag{25}$$

where $w^a_{A,21}$ is the vertical displacement of point D of layer a (Fig. 7) for the 21 E_4 finite-element mesh, and $w^a_{A,k}$ is the value corresponding to the k finite-element mesh. The results are presented for two load levels, $\lambda = 10$ and $\lambda = 54$, using elements E_4 with 3rd degree polynomial interpolation. The load level $\lambda = 54$ represents the collapse load of the structure which occurs due to the tensile failure of timber fibres at the bottom part of the cross-section.

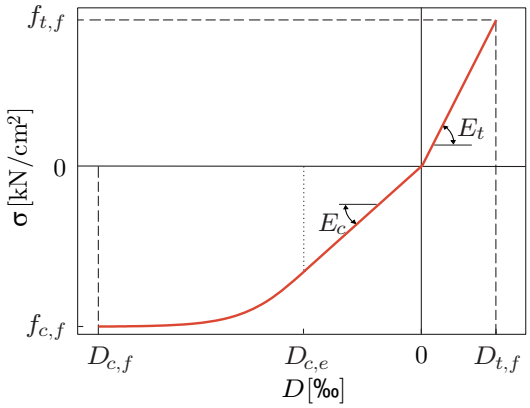

Figure 8: Timber stress-strain relationship [43].

Fig. 10 shows the plots of the relative error of vertical displacement w_D vs. the number of elements for load levels $\lambda = 10$ and $\lambda = 54$ for (a) a rigid connection ($C = 1000$ kN/cm^2) and (b) a non-linear contact in the normal direction according to Fig. 9(b). An excellent convergence can be observed for both load levels and both types of the connection model. The mesh of only 3 finite elements is sufficient to obtain the results within the 0.25% error.

4.2. The influence of ζ

We added a new parameter ζ in Eqs. (9) to a definition of the mean contact surface vectors. Here we study the effect of ζ on the vertical and transverse displacement of layers. The analysis is carried out for two similar cases. We consider a two-layer beam whose geometrical and material properties are identical to those of Fig. 4. The boundary conditions and the load arrangement are, however, different, see Figs. 11 and 13. In the first numerical case, the beam is subject to transverse forces $\lambda P_1 = \lambda \cdot 10$ kN and $\lambda P_2 = \lambda \cdot 5$ kN, and an axial force $\lambda P_3 = \lambda \cdot 50$ kN at the free end of the upper layer applied at the contact surface (see Fig. 11). In the second numerical case, we replaced the axial force with a bending moment $\lambda M = \lambda \cdot 50$ kNcm (see Fig. 13). A bilinear constitutive relationship in the normal direction is considered in both cases, with a tangen-

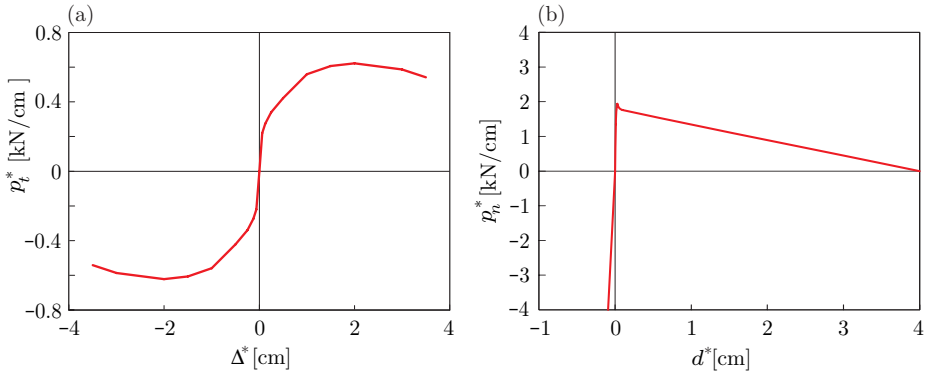

Figure 9: (a) Non-linear contact relationship in tangential direction $\mathbf{e}_t^*$, (b) Non-linear contact relationship in normal direction $\mathbf{e}_n^*$ [44].

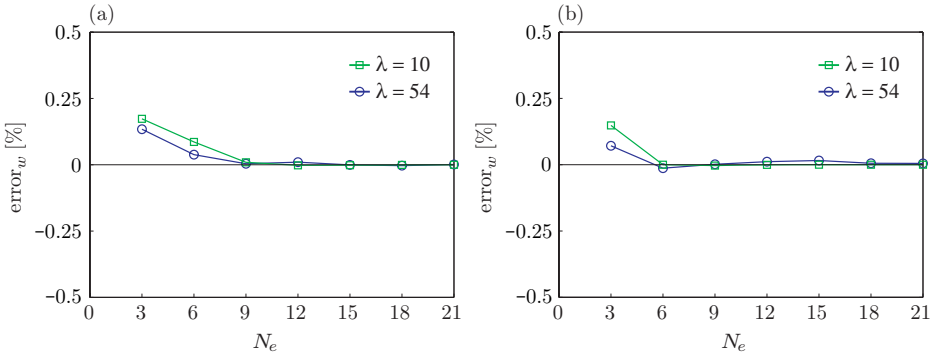

Figure 10: Relative error of vertical displacement w_D vs. number of elements for load levels $\lambda = 10$ and $\lambda = 54$: (a) rigid normal connection ($C = 1000$ kN/cm^2), and (b) non-linear contact in the normal direction (as in Fig. 9(b)).

tial moduli in compression (tension) $C_c = 100$ kN/cm^2 ($C_t = 1$ kN/cm^2), while a linear constitutive relationship in the tangential direction is assumed with $K = 1$ kN/cm^2.

Table 2 displays the results for various ζ. There we compare transverse and axial displacements of the layers at the midspan and at the unsupported end of the upper layer for different values of ζ. The relative difference between the results appears to be rather small. Fig. 12 shows the deformed shape of the

axially loaded two-layer beam for the load level $\lambda = 100$ assuming $\zeta = 0.5$. As seen, there exists a significant relative motion of the contact surfaces in both normal and tangential directons.

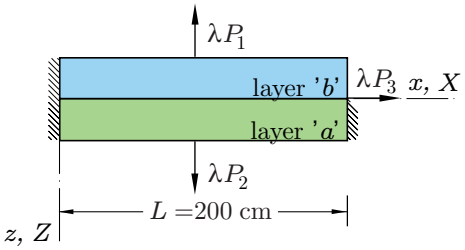

Figure 11: Geometry, loading and supports of axially loaded two-layer beam.

Table 2: Axially loaded two-layer beam. Comparison of results for different ζ at $\lambda = 100$.

ζ	$w^a[L/2]$	$w^b[L/2]$	$u^a[L/2]$	$u^b[L/2]$	$w^b[L]$	$u^b[L]$
0.50	-3.06 cm	-13.22 cm	2.59 cm	10.69 cm	-11.45 cm	25.87 cm
0	-1.98%	0.17%	-1.15%	-0.11%	0.45%	0.03%
0.25	-1.01%	0.16%	-0.75%	-0.08%	0.38%	0.04%
0.75	-0.01%	-0.32%	1.05%	0.12%	-0.69%	0.15%
1.00	0.30%	-0.59%	2.06%	0.24%	-1.28%	0.22%

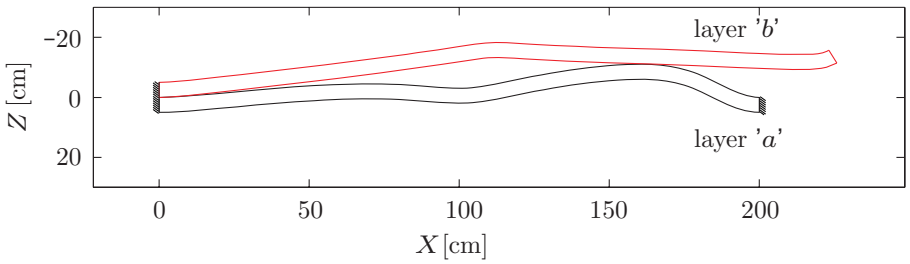

Figure 12: The deformed shape of axially loaded two-layer beam. Load level $\lambda = 100$, $\zeta = 0.5$.

Table 3 presents the analogous results of the beam when loaded with the bending moment at its free end. We compared transverse and vertical displace-

ments of each beam layer at beam midspan and at the unsupported end of a beam for different values of ζ. As in the previous case the relative difference between the results is small again. Fig. 14 presents the deformed shape for the moment level $\lambda = 150$ and $\zeta = 0.5$. Again, a severe relative motion of the contact surfaces takes place both in normal and tangential directons.

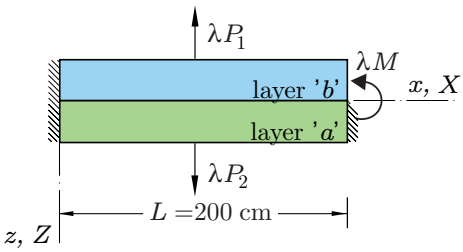

Figure 13: Geometry, loading and supports of two-layer beam subject to bending moment.

Table 3: A two-layer beam subject to bending moment. Comparison of results for different ζ at $\lambda = 150$.

ζ	$w^a[L/2]$	$w^b[L/2]$	$u^a[L/2]$	$u^b[L/2]$	$w^b[L]$	$u^b[L]$
0.50	-11.71 cm	-32.62 cm	-0.76 cm	-3.26 cm	-24.50 cm	-18.04 cm
0	-0.02%	-0.01%	-0.22%	0.28%	-0.26%	0.95%
0.25	-0.01%	-0.00%	-0.16%	0.14%	-0.08%	0.45%
0.75	0.02%	0.01%	0.20%	-0.09%	0.05%	-0.31%
1.00	0.01%	0.02%	0.54%	-0.12%	-0.32%	-0.63%

4.3. Validation of the model

The model is validated by the laboratory results of Ansourian [39] for the continuous steel-concrete composite beam and the numerical results of Čas et al. [44]. The model in [44] assumes a geometrically linear theory of composite beams. Loading, supporting and geometrical properties of the beam are shown in Fig. 15.

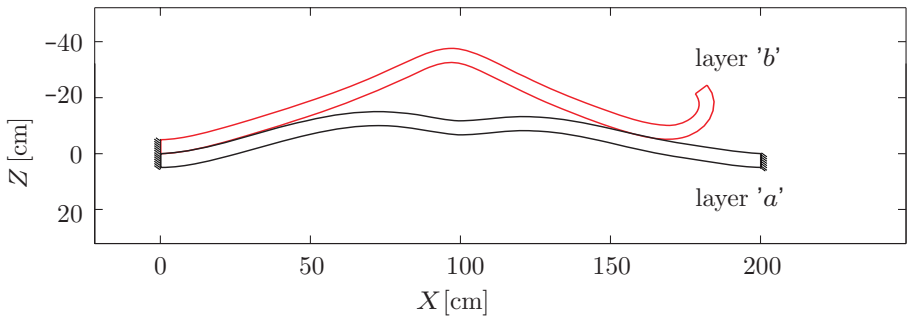

Figure 14: The deformed shape of two-layer beam subject to bending moment. Load level $\lambda = 150$, $\zeta = 0.5$.

The concrete part of the cross-section is reinforced both at the top and at the bottom region with the steel reinforcement bars, yet the reinforcement differs in the areas of sagging and hogging moments: $A_{\text{top}}^{\text{sag}} = 0$ cm^2, $A_{\text{bottom}}^{\text{sag}} = 1.6$ cm^2, $A_{\text{top}}^{\text{hog}} = 8.0$ cm^2 and $A_{\text{bottom}}^{\text{hog}} = 3.16$ cm^2.

Fig. 16 presents the material models employed in the analysis. The three-linear constitutive model is considered for steel (Fig. 16(a)), where $E_s = 21000$ kN/cm^2, $E_{sh} = 0.008E_s$, $f_y^{\text{flange}} = 27.7$ kN/cm^2, $f_u^{\text{flange}} = 42.1$ kN/cm^2, $f_y^{\text{web}} = 34.0$ kN/cm^2, $f_u^{\text{web}} = 44.0$ kN/cm^2, $f_y^{\text{reinforcement}} = 43.0$ kN/cm^2, $f_u^{\text{reinforcement}} = 53.3$ kN/cm^2 and $D_{sh} = 0.012$. The model of Desayi and Khrishnan [45] (Fig. 16(b)) is assumed for concrete, where $f_{cm} = 3.0$ kN/cm^2, $D_{c1} = -2.25$ ‰ and $D_{cu} = -21$ ‰. The non-linear mean slip – tangential traction force relationship is assumed as proposed by Ollgaard et al. [4] (Fig. 16(c)). The material parameters of their model (Fig. 16(c)) are: $\alpha = 0.558$, $\beta = 10$ cm^{-1} and $p_{t,max}^* = 6.53$ kN/cm.

There are several mean uplift – normal traction force relationships available in literature. The graphs of linear, bi-linear [31] and non-linear [33] contact models often used in research are depicted in Fig. 16(d).

Fig. 17 shows some comparisons between the results of Ansourian [39], Čas et al. [44] and the present model. There the vertical displacements of point 1 (w_1) and point 2 (w_2) for a normal rigid connection ($C = 1000$ kN/cm^2) are

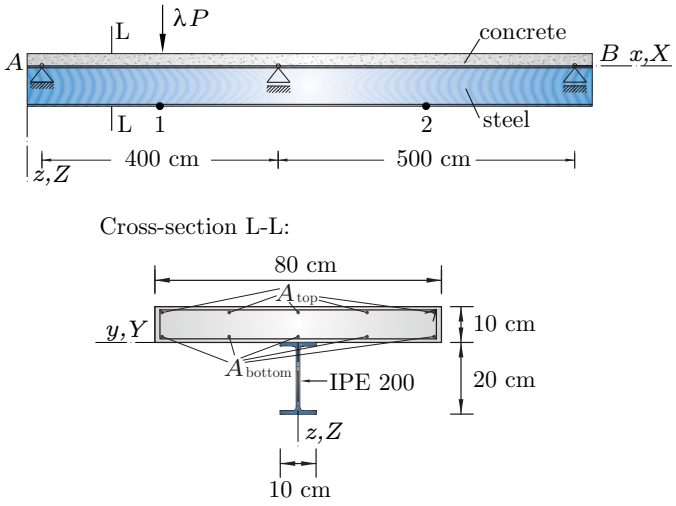

Figure 15: Loading, supports and geometrical properties of the steel-concrete continuous beam [39].

compared. 9 E_4 element meshes were employed in our numerical calculations. The comparisons between the results show that the stiffness, ductility and load capacity are well described by the present model. The ultimate load 192 kN was estimated particularly well being only slightly less than the one obtained experimentally (196 kN). Results also indicate that the chosen number of studs results in a very stiff contact in the normal direction, as the numerical results for the loading capacity and ductility for the rigid contact ($C = 1000$ kN/cm) compare best with the experimental ones. The comparisons with Čas et al. [44] also reveal a very good agreement. These results also indicate that displacements, rotations and deformations are rather small quantities. This is due to the experimental fact that the structure collapsed shortly after the simultaneous localization of deformations in the concrete slab and a huge development of plastic deformations of steel took place [39]. The same mechanism of collapse is established by the present numerical model.

We have also studied the effect of the contact model in the normal direction $\mathbf{e}_n^*$ on the load-deflection curve. We employed two linear (with the tangential

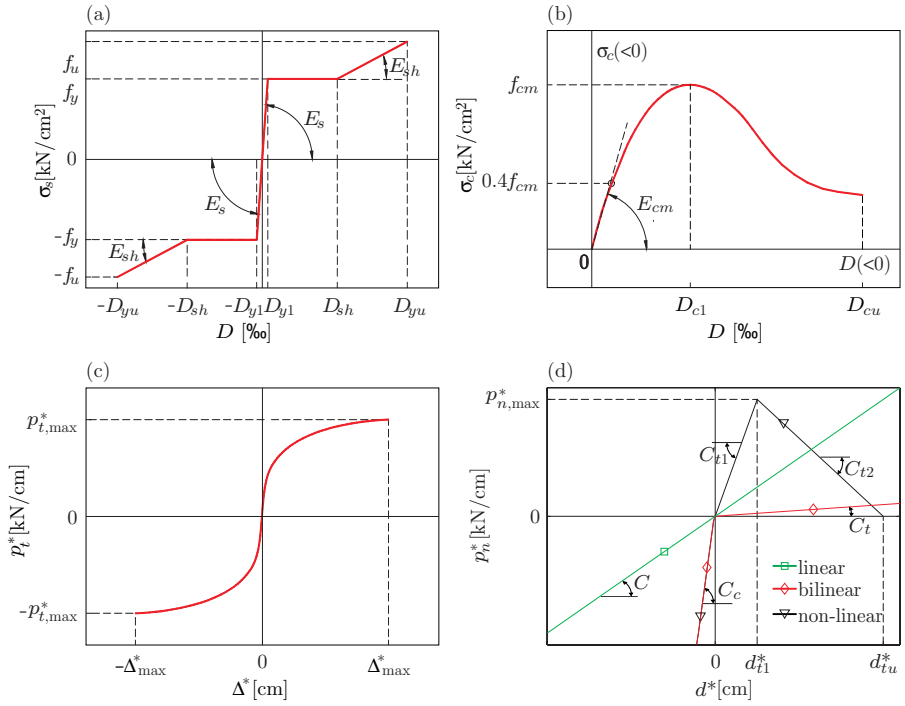

Figure 16: Material models of: (a) steel and reinforcement, (b) concrete, (c) mean slip – traction force in tangential direction $\mathbf{e}_t^*$, (d) mean uplift – traction force in normal direction $\mathbf{e}_n^*$.

moduli $C = 1$ kN/cm^2 and $C = 1000$ kN/cm^2), a bi-linear ($C_c = 100$ kN/cm^2 and $C_t = 1$ kN/cm^2) and a non-linear relationship ($C_c = 100$ kN/cm^2, $C_{t1} = 40$ kN/cm^2, $C_{t2} = 13.33$ kN/cm^2, $d^*_{t1} = 0.25$ cm and $d^*_{tu} = 1$ cm).

The comparisons are shown in Fig 18. It is clearly seen from Fig. 18 that a lower rigidity decreases both the ultimate loading and the ductility of the beam. It can also be observed that the choice of the contact model in the normal direction has only a minor effect on the load-deflection curve in the linear regime of deformation.

The choice of the constitutive law in the normal direction $\mathbf{e}_n^*$ on tractions, p_t^* and p_n^*, is finally studied. For the sake of better graphic representation, we consider the 20 finite-element mesh with E_4 elements, although even a much

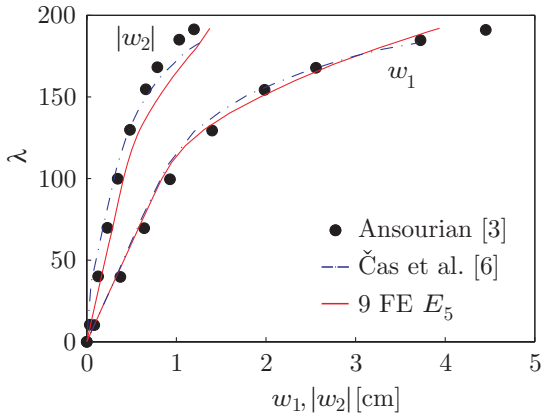

Figure 17: Comparison of load-deflection curves of vertical displacement at points 1 and 2.

smaller number of finite elements would give sufficiently accurate results. A detailed analysis shows a negligible effect of the contact model on static quantities, as clearly seen from Fig. 19, where the variation of bending moments M^a and M^b along the reference axis of the beam is depicted.

The effect of different contact laws on p_t^* and p_n^* is presented in Fig. 20. As seen from Fig. 20(a), the effect on p_t^* is minor. This is not the case with p_n^*, however, where a flexible type of connection may result in a substantially different p_n^* compared to the rigid connection. Note, however, that major differences are localized around the point of application of the load.

5. Conclusions

We have introduced the mathematical model of the geometrically exact two-layer planar composite beam whose material properties and the behaviour of connection are fully non-linear. The model is capable of describing large displacements and rotations as well as large slip and uplift between the layers.

The governing equations of the model have been discretized by the strain-based finite element mehod where only the strain measures, the extensional strain and the curvature of the axis, are interpolated. The formulation enables us

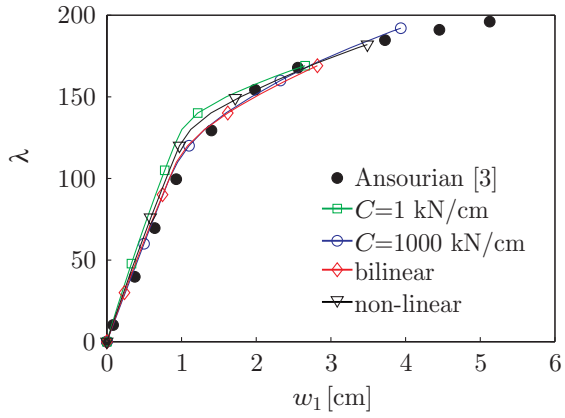

Figure 18: Load-deflection graphs of vertical displacement at point 1, w_1 vs. load factor, λ, for various normal contact laws.

to obtain the solution for arbitrary frame-like structures made up of individual composite beams. Both slip and uplift are allowed between the layers. The results may well depend on the nature of the contact law which has to be referred to the rotated normal and tangential directions of the deformed contact surface.

Material properties of layers are also assumed non-linear and easily include such combinations as timber-timber, timber-concrete and steel-concrete, being often used in structural engineering.

Numerical analyses indicate that the present strain-based finite element formulation:

- is very accurate in both linear and non-linear regime, so that only a few finite elements E_4 are needed to obtain almost exact results;
- is computationally efficient, because its p- and h-convergence is fast and practically monotonous, the overall iterative solution algorithm very robust, and the results reliable;
- is thus highly convenient for the analysis of stiffness, ductility, load capacity and collapse mode of civil engineering composite structures.

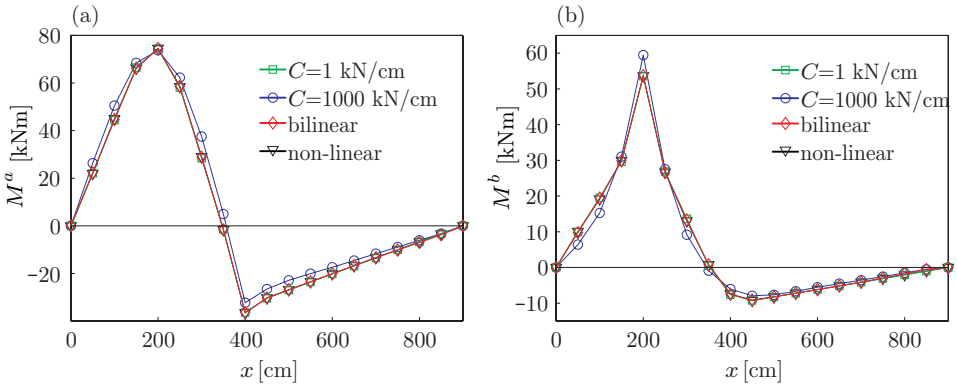

Figure 19: Effect of different normal contact laws on M^a and M^b.

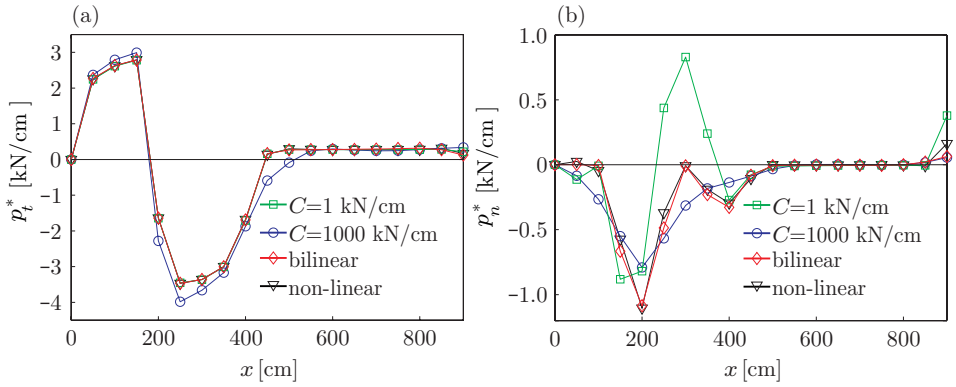

Figure 20: Effect of different normal contact laws on p_t^* and p_n^*.

Acknowledgment

The work of Aleš Kroflič was supported by the Slovenian Research Agency through the grant 1000-07-310191. The support is gratefully acknowledged.

References

[1] B. Čas, M. Saje, I. Planinc. *Non-linear finite element analysis of composite planar frames with an interlayer slip*, Comput. Struct. 2004;82:1901–1912.

[2] A. Ayoub. *A force-based model for composite steel-concrete beams with partial interaction*, J. Constr. Steel Research. 2005;61(3):387–414.

[3] H. Robinson, K. S. Naraine. *Slip and uplift effects in composite beams*, Int. Conf. Comp. Constr. Steel Conc., Proc. Eng. Found. Conf. ASCE, New England College, Henniker, New Hampshire, 487–497, 1988.

[4] J. G. Ollgaard, R. G. Slutter, J. W. Fisher. *Shear strength of stud connectors in lightweight and normal weight concrete*, AISC Eng. J. 1971:55–64.

[5] R. Salari, E. Spacone, P. B. Shing, D. M. Frangopol. *Nonlinear analysis of composite beams with deformable shear connectors*, ASCE J. Struct. Eng. 1998;124(10):1148–1158.

[6] A. Kryžanowski, S. Schnabl, G. Turk, I. Planinc. *Exact slip-buckling analysis of two-layer composite columns*, Struct. Eng. Mech. 2006;22(3):263–278.

[7] G. Fabbrocino, G. Manfredi, E. Cosenza. *Non-linear analysis of composite beams under positive bending*, Comput. Struct. 1999;70:77–89.

[8] R. Xu, Y. F. Wu. *Two-dimensional analytical solutions of simply supported composite beams with interlayer slips*, Int. J. Solids Struct. 2007;44:165–175.

[9] H. Granholm. *On composite beams and columns with special regard to nailed timber structures*, Trans. No. 88, Chalmers University of Technology, Goeteborg, Sweden (in Swedish), 1949.

[10] N. M. Newmark, C. P. Siess, I. M. Viest. *Tests and analysis of composite beam with incomplete interaction*, Proc. Soc. Exp. Stress Analy. 1951;9:75–92.

[11] P. F. Pleshkov. *Theoretical studies of composite wood structures*, Soviet Union (in Russian), 1952.

[12] F. Stüssi. *Zusammengesetze Vollwandträger*, International Association for Bridge and Structural Engineerig (IABSE) 8, 249–269, 1947 (in German).

[13] A. O. Adekola. *Partial interaction between elastically connected elements of a composite beam*, Int. J. Solids Struct. 1968;4(11):1125–1135.

[14] M. A. Bradford, R. I. Gilbert. *Composite beams with partial interaction under sustained loads*, ASCE J. Struct. Eng. 1992;118(7):1871–1883.

[15] A. Kroflič, I. Planinc, M. Saje, B. Čas. *Analytical solution of two-layer beam including interlayer slip and uplift*, Struct. Eng. Mech. 2010;34(6):667–683.

[16] G. Manfredi, G. Fabbrocino, E. Cosenza. *Modeling of steel-concrete composite beams under negative bending*, J. Eng. Mech. 1999;125(6):654–662.

[17] S. Schnabl, I. Planinc, M. Saje, B. Čas, G. Turk. *An analytical model of layered continuous beams with partial interaction*, Struct. Eng. Mech. 2006;22(3):263–278.

[18] R. Betti, A. Gjelsvik. *Elastic composite beams*, Comput. Struct. 1996;59(3):437–451.

[19] B. Čas, M. Saje, I. Planinc. *Non-linear analysis of composite steel-concrete beams with incomplete interaction*, Steel Comp. Struct. 2004;4(6):489–507.

[20] N. Gattesco. *Analytical modeling of nonlinear behavior of composite beams with deformable connection*, J. Constr. Steel Res. 1999;52:195–218.

[21] T. Hozjan. *Nonlinear analysis of composite planar structures exposed to fire*, University of Ljubljana, Faculty of Civil and Geodetic Engineering, Doctoral thesis (in Slovene); 2009.

[22] H. R. Milner, H. H. Tan. *Modelling deformation in nailed, thin-webbed timber box beams*, Comput. Struct. 2001;79:2541–2546.

[23] I. Planinc, S. Schnabl, M. Saje, J. Lopatič, B. Čas. *Numerical and experimental analysis of timber composite beams with interlayer slip*, Eng. Struct. 2008;30:2959–2696.

[24] H. A. Rasheed, S. Pervaiz. *Bond slip analysis of fiber-reinforced polymer-strengthened beams*, J. Eng. Mech. 2002;1:78–86.

[25] R. Seracino, D. J. Oehlers, M. F. Yeo. *Partial-interaction flexural stresses in composite steel and concrete bridge beams*, Eng. Struct. 2001;23:1186–1193.

[26] Y. C. Wang. *Deflection of steel-concrete composite beams with partial interaction*, ASCE J. Struct. Eng. 1998;124(10):1159–1165.

[27] G. Ranzi, M. A. Bradford. *Direct stiffness analysis of a composite beam-column element with partial interaction*, Comput. Struct. 2007;85(15–16):1206–1214.

[28] G. Ranzi, A. Dall'Asta, L. Ragni, A. Zona. *A geometric nonlinear model for composite beam with partial interaction*, Eng. Struct. 2010;32:1384–1396.

[29] F. Kamiya. *Buckling of sheated walls: Nonlinear analysis*, ASCE J. Struct. Eng. 1987;114(3):625–641.

[30] H. Y. Rassam, J. R. Goodman. *Buckling behavior of layered wood columns*, Wood Science. 1970;2(4):238–246.

[31] F. Gara, G. Ranzi, G. Leoni. *Displacement based formulations for composite beams with longitudinal slip and vertical uplift*, Int. J. Numer. Methods Eng. 2006;65(8):1197–1220.

[32] G. Ranzi, F. Gara, P. Ansourian. *General method of analysis for composite beams with longitudinal and transverse partial interaction*, Comput. Struct. 2006;84:2373–2384.

[33] G. Alfano, M. A. Crisfield. *Finite element interface models for the delamination analysis of laminated composites: mechanical and computational issues*, Int. J. Numer. Methods Engng. 2001;50:1701–1736.

[34] B. J. Daniel, M. Crisinel. *Composite slab behavior and strength analysis. Part I: Calculation procedure*, ASCE J. Struct. Eng. 1993;119(1):16–35.

[35] A. Dall'Asta, A. Zona. *Comparison and validation of displacement and mixed elements for the non-linear analysis of continuous composite beams*, Comput. Struct. 2004;82:2117–2130.

[36] A. Ayoub, F. C. Filippou. *Mixed formulation of nonlinear steel-concrete composite beam element*, ASCE J. Struct. Eng. 2000;126(3):371-381.

[37] I. Planinc, M. Saje, B. Čas. *On the local stability condition in the planar beam finite element*, Struct. Eng. Mech. 2001;12(5):507–526.

[38] U. A. Girhammar, V. K. A. Gopu. *Composite beam-columns with interlayer slip - exact analysis*, ASCE J. Struct. Eng. 1993;119(4):1265–1282.

[39] P. Ansourian. *Experiments on continuous composite beams*, Proc. Inst. Civ. Eng. 1981;71(Part 2):25–51.

[40] E. Reissner. *On one-dimensional finite-strain beam theory: The plane problem*, J. App. Math. Phys. (ZAPM) 1972;23:795–804.

[41] G. N. Wells, R. De Borst, L. J. Sluys. *A consistent geometrically non-linear approach for delamination*, Int. J. Num. Meth. Eng. 2002;54:1333–1355.

[42] A. Kroflič, I. Planinc, M. Saje, G. Turk, B. Čas. *Non-linear analysis of two-layer timber beams considering interlayer slip and uplift*, Eng. Struct. 2010;32(6):1617–1630.

[43] R. Pischl. *Holzbau mit kritischen betrachtungen und neuen vorschlägen zur bemessungnach theorie 1. und 2. ordnung*, Institut für Stahlbau, Holzbau und Flächentragwerke, Technische Univerität Graz, 1980.

[44] B. Čas. *Non-linear analysis of composite beams considering slip between the layers*, University of Ljubljana, Faculty of Civil and Geodetic Engineering, Doctoral thesis (in Slovene); 2003.

[45] P. Desayi, S. Krishnan. *Equation for the stress-strain curve of concrete*, J. Am. Conc. Inst. 1964;61–22.